ION-CONCENTRATION POLARIZATION REGIMES FOR NANOCAPILLARY ARRAY MEMBRANES

Undergraduate Senior Honor Thesis

Presented in Partial Fulfillment of the Requirements for Graduation with Distinction in

The Department of Mechanical Engineering

By Wenqin He

July 27th, 2012

The Ohio State University

Columbus, Ohio 43210

Oral Defense Committee Members:

Dr Shaurya Prakash, Advisor

Dr. Robert Siston

Abstract

The current methods for water desalination based on electrical approaches that use membranes for ion filtration can be inefficient in terms of energy efficiency. One reason for energy inefficient desalination is the concentration polarization (CP) region at the membrane-solution interface. A better understanding towards CP is essential in improving the process and increasing the efficiency of the membrane separation processes. This work reports on characterization and identification of CP regimes for a potassium phosphate buffer through model nanocapillary array membranes or NCAMs for sub-1V operation conditions. The low operating voltage range is chosen to minimize faradaic reactions and complement other research in the Prakash group towards low-energy consuming water desalination. Three nanopore sizes in NCAMs (10 nm, 50 nm, 100 nm) were used under different bias (10 mV - 750 mV) and concentration (0.2 mM, 1 mM, 10 mM) at pH 7. CP regime is identified and compared to previous reports for CP in membrane system with electrokinetically driven flows. The results indicate that the voltage for onset of the CP regime increases with smaller pore size and lower buffer concentration.

Acknowledgments

I would like to thank my adviser, Professor Shaurya Prakash, for all the guidance, encouragement and support he has given me over the past year. Without his help, this project would not have been possible.

I would also like to thank Karen Bellman for her assistance and guidance that helped me in data analysis and thesis writing, and Dr. Harvey Zambrano for his insight that helped me in understanding the science behind this project.

Special thanks to Professor Robert Siston for his endless support.

This research is supported by the Microsystems and Nanosystems Lab of The Ohio State Univeristy, and an undergraduate honors research scholarship awarded by the College of Engineering.

Table of Contents

List of Figures

List of Tables

1. Introduction

1.1 Water crisis and current water desalination technology

1.1.1 Fresh water and water crisis

Fresh water is essential to life. Besides the fresh water that is needed for human survival and agricultural uses, tremendous amounts of fresh water are also required for industrial operations. From Figure 1, approximately 41% of freshwater withdrawals are used for thermoelectric cooling and 37% for irrigation in the United States [1].

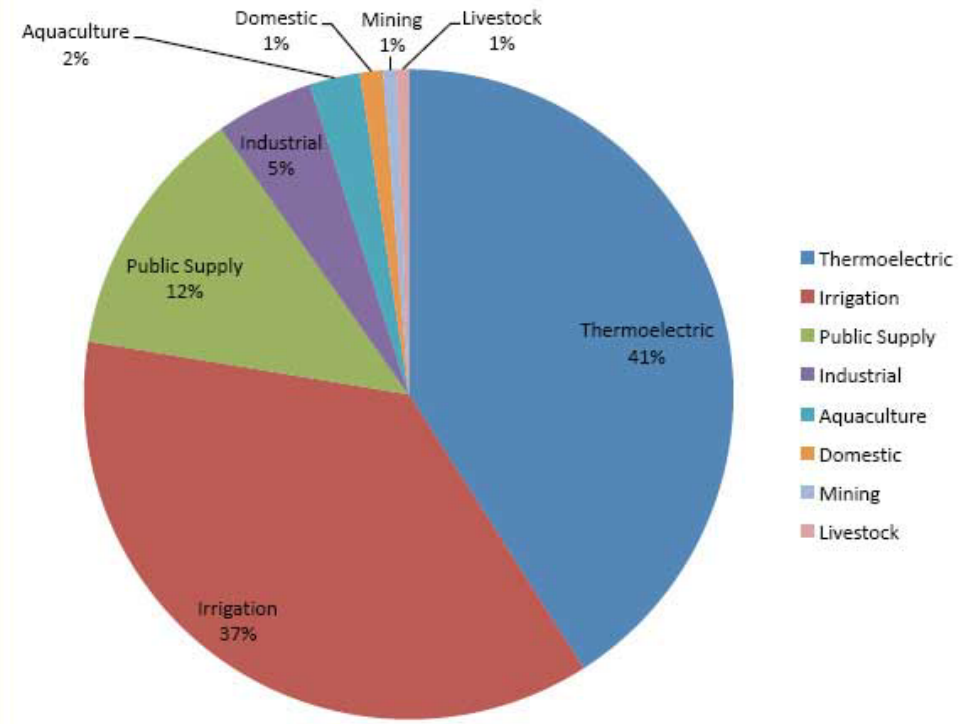

Figure 1. Total fresh water withdrawals in the United States in 2005 [1]

Due to the importance of water as a resource for modern society, it is essential to evaluate the sustainability of current water usage. Water shortage will become a great issue in the near future. In the United States, many regions, such as the west of Texas and south of Georgia, have already been suffering with severe drought since the early 1950s [2]. While climate is one of the factors responsible for the disaster, lack of access to sufficient fresh water supplies and

population growth also contribute to this issue. Only 2.5% of water on the earth is fresh water, and saline sea water accounts for the rest of the 97.5%. Among the 2.5%, 68.9% of fresh water is locked in ice caps and glaciers that cannot be utilized directly [1]. With such limited fresh water resources available, the rapid growth of the world population at 1.1% per year (75 million people/year) [3] undoubtedly further worsens the water crisis. In 2010, nearly 2.4 billion people live in water-scare regions [4], where basic daily freshwater requirements cannot be satisfied. Figure 2 shows the areas where intense water usage stresses were experienced in 2010. Improving the effectiveness of current water purification technologies and developing alternative methods to increase the current fresh water supply become essential to alleviate our fresh water shortages. Desalination of saline water may be one of the most perspective technologies to produce sustainable fresh water supply in the future [5].

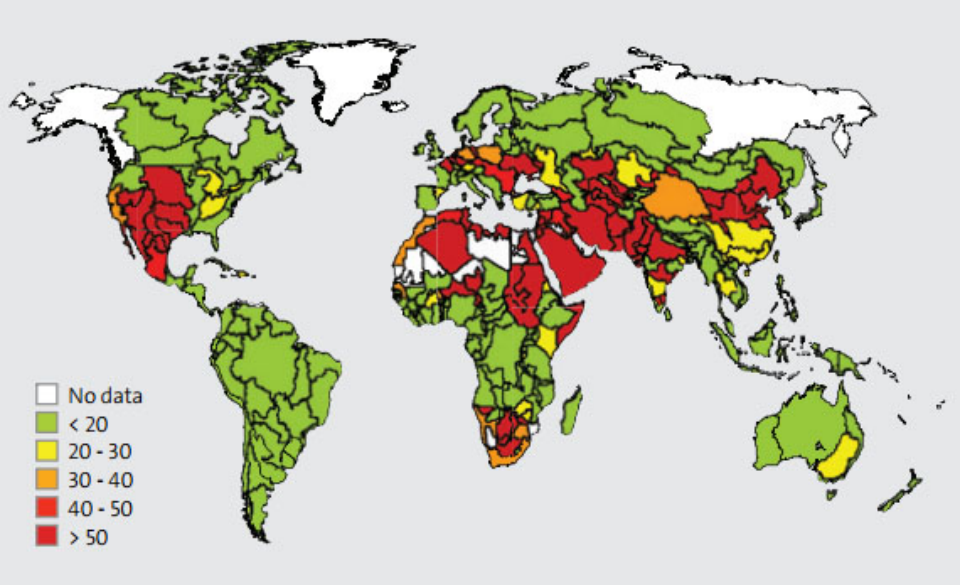

Figure 2. Water stressed areas for 2010. The number on the legend represents the percent of total renewable water withdrawn. The red area indicates an intense stress while the green area indicates a mild one [4]

1.1.2 Evolution of water desalination

Although the natural water cycle transfers saline water into the fresh water as precipitates, the process period is unpredictable and uncontrollable, it cannot serve as an effective fresh water supply to solve the current water crisis and meet the high volume demand. Industrial water desalination plants offer an effective method of augmenting the water supply. Desalination is the process that extracts fresh water from saline water, and was invented first by Greek sailors who used wool condensators to collect fresh water on board ships around 5th century B.C. [6]. The early age desalination techniques were mainly small scale distillation processes for navy and sailors. In 1881, the first commercial desalination plant was installed in Tigne, Malta to supply water to the local community. With the development of the semipermeable membrane in the mid 19th century, membrane based separation was brought to the stage [6].

1.1.3 Current saline desalination technology and its challenges

Current saline desalination includes thermal processing and membrane processing. The flow diagrams in Figure 3 describe general procedures and major characteristics of each desalination method.

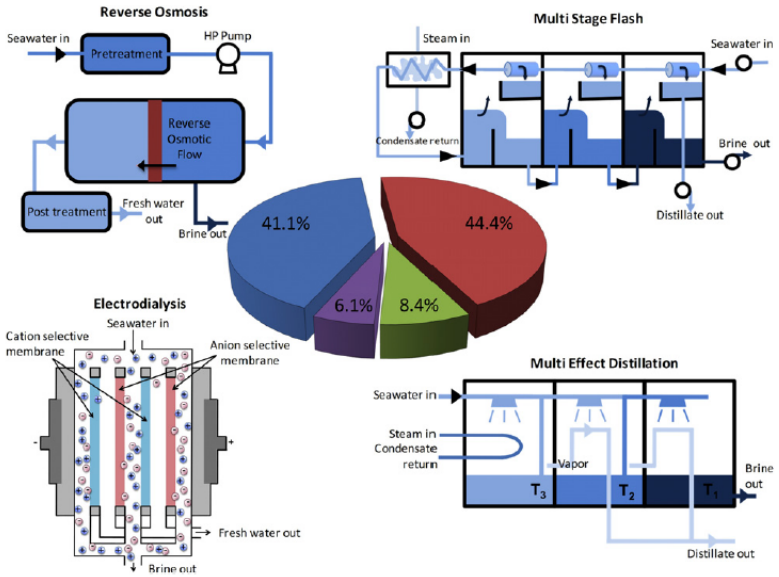

Figure 3. Current desalination technology and their global installed capacity distribution [7]

Thermal distillation is exploited by countries in the middle-east due to their easily accessible fossil fuel resource, and the high salinity and high temperature of the saline water in Persian Gulf and Gulf of Oman has high potential to cause membrane fouling [8]. However, outside the middle-east area where energy resource is limited, the installation capacity of membrane-based desalination plants has been steady increased from 2001 [8].

Since energy has become a big issue throughout the world, it is urgent to examine the feasibility of current and new saline desalination processes. Traditional distillation methods such as multi-stage flash (MSF) and multi-effect distillation (MED) in Table 1 require approximately 300 kJ/L energy for heating while achieving around 20% conversion to fresh water. The reverse osmosis process (RO) needs up to 25.2 kJ/l energy without any heat consumption to achieve 20-50% of conversion as well. Therefore, membrane processing is more energy efficient than traditional distillation methods [7] [9].

Table 1. Energy table for major saline water desalination technology [10]

Process	MSF	MED/TVC	RO
Heat Consumption(kJ/L)	290	145-390	--
Electricity Consumption (kJ/L)	10.8-18	5.4-9	9-25.2
Estimated Total Energy Consumption (kJ/L)	300.8-308.8	150.9-399	9-25.2
Conversion to the fresh water (recovery)	10-25%	23-33%	30-50%

The biggest challenge for membrane processing is membrane fouling due to the scale formation and deposition [11]. In order to mitigate this problem, excess energy consumption is required in the pre-treatment step which raises the overall energy demand. Concentration polarization phenomena that can cause membrane fouling needs to be eliminated systematically in order to improve operation lifetimes of the membranes, optimize system performances, as well as decrease the excess energy consumptions. Furthermore, any CP mitigation methods must

involve minimal energy and material consumptions so as not to change the system energy budget significantly.

1.2 Membrane separation

Membrane separation processes are becoming increasingly important due to low-energy consumption and easy scale-up [12]. Membrane acts as a semipermeable barrier to achieve separation by limiting the rate of movement of various molecules between two fluid phases which are usually miscible [13]. The solution-diffusion model is widely used to characterize the flow mechanism in membrane. The permeant substances diffuse through membrane at different rates based on their diffusivity within the membrane, membrane pore size, and concentration of permeant substances on either side of the membrane [14]. When electric filed is applied to the system, the flux of solute will be affected by various factors. A single direction transfer phenomenon model is defined by 1-D Nernst-Planck equation

$$\boldsymbol{J_i = -D_i \frac{\partial c_i}{\partial x} + c_i \nu - \frac{FD_i}{RT} z_i c_i \frac{\partial \phi}{\partial x}} \quad (1)$$

where J_i is the flux of *i*th speicie, D_i is the diffusivity , c_i is the molar concentration of *i*th speicie, ν is bulk fluid velocity, R is unversal gas constan, T is absolute temperature, F is Faraday's constant, z_i is the valence of species and ϕ is the electrical potential. The ions transport phenomenon of the membrane separation system with electric field is determined by diffusion term $\boldsymbol{D_i \frac{\partial c_i}{\partial x}}$, convection term $\boldsymbol{c_i \nu}$ and especially potential ditrubution term $\boldsymbol{\frac{FD_i}{RT} z_i c_i \frac{\partial \phi}{\partial x}}$ [15].

1.3 Concentration polarization

1.3.1 Electric double layer

Membrane selectivity is determined by pore size, surface chemistry and surface charge. Small, uncharged or nonpolar particles and molecules are more favorably to pass through the nanopore compared to the larger, charged or polar one. Besides the physically manufactured pore

diameter, the formation of electric double layer (EDL) due to the surface charge and the surface chemistry also helps to control the separation by selectively reject ions. The electrical double layer (EDL) is a specific charge distribution at the liquid-solid interface: the fixed surface charges on the solid are compensated by mobile counterions in solution [16].

The surface charge at the solid/liquid interface attracts counter ions in the solution to form stern layer and diffuse layer as illustrated in Figure 4. The stern layer is usually described as immobilize thin layer of a few Angstroms thick [17], while the diffuse layer is the mobilized one with freer ion movements.

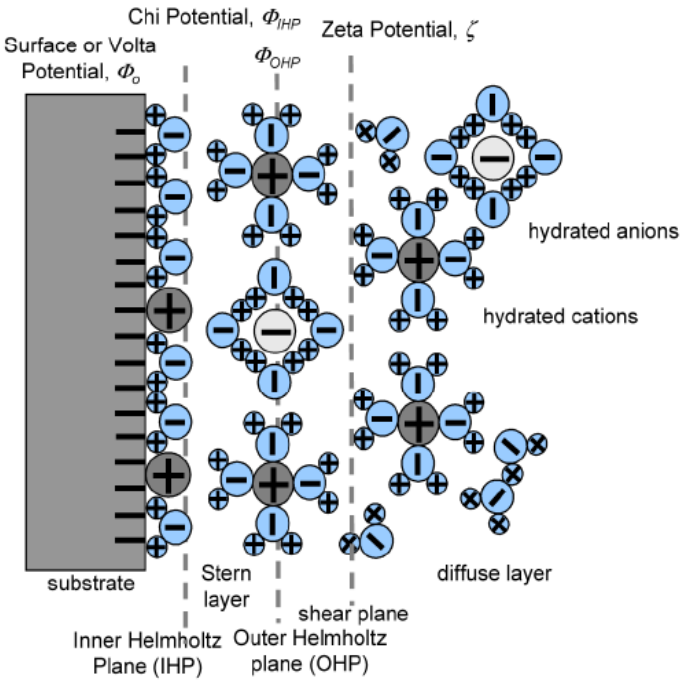

Figure 4. Schematic diagram of electric double layer (EDL) [15]

Combining the Boltzmann distribution with the Poisson equation, the shielding length of EDL is defined as

$$\lambda_D = \sqrt{\frac{\varepsilon_e RT}{F^2 z^2 c_i}} \tag{2}$$

where ε_e is electric permittivity of the medium, R is gas constant, F is Faraday's constant, z is integer valence number and c_i is concentration of specie i. This is what usually called Debye length. For symmetric monovalent electrolyte, Debye length is about 0.3-530 nm in concentration ranging from 0.33 μM to 1 M corespondingly [10]. The overall thickness of EDL can be estimated as five time the Debye length. The value of λ_D is dependent on the concentration of electrolyte, where high concentration generates a thinner debye length while low concentration creates a thicker layer for ion shielding.

For a cylindrical interface, if an overlapping exists where EDL interacts with each other, the pore channels preferentially transport the ions that make up the overlapped layers. For example, if the major ions in the diffuse layer are cations when EDL overlaps a membrane pore channel, then anions can transfer through the pore easily while cations can be rejected back to the bulk solution. The dimensionless parameter κa was used to determine the EDL interaction within the pore, where κ is inverse Debye length, and a is pore diameter. For $\kappa a > 1$, the EDL is non-overlapping, so that electromigration dominates the flow transport; for $\kappa a \ll 1$ the EDL overlaps, so that electroosmosis dominates the flow [10] [15]. The overlapping of EDL accelerates the accumulation of ions near membrane to initial CP. For small scale, the decrease of pore size increases the volume to surface area ratio which increases the influence of the EDL to the system.

1.3.2 Formation of concentration polarization

The exsistence of EDL and its property of overlapping helps to achieve membrane selectivity of ions. CP refers to the accumulation of solute at the surface of the membrane, causing the solute concentration at the membrane wall to be greater than that of the bulk feed

solution [18]. In addition, finite surface charge at the membrane surface also allows for adsorption of ions to the membrane that contributing to the formation of the CP region.

Figure 5 demonstrates the concentration distribution on either side of membrane when concentration polarization is present. If the flow goes across the membrane from right (high ion concentration) to the left, the ion transport causes a lower concentration on the righ side membrane ($C_{0+} < C_{b+}$) and higher concentration in left side of membrane ($C_{0-} > C_{b-}$) [19]. As a result, the decrease in local concentration difference between the membrane surface and the solution leads to solvent flux decrease that lowers the effectiveness of the membrane to generate the end product in water desalination.

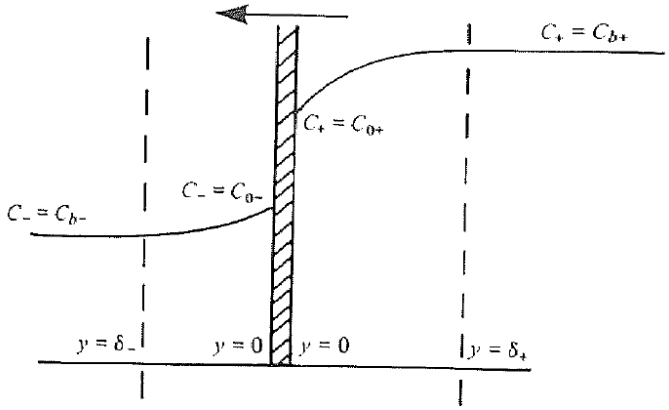

Figure 5. The formation of concentration polarization. Note that the +,- signs indicate the right and left side respectively [9]

Beginning with van't Hoff formula for osmotic pressure,

$$\boldsymbol{\pi = cRT} \tag{3}$$

Where π is osmotic pressure, c is molar concentration, R is gas constant and T is temperature. When the concentration near the membrane increases, the local osmotic pressure will also go up.

$$\boldsymbol{\Delta\pi = \beta\pi_1 - \pi_2} \tag{4}$$

Where β is the ratio of salt concentration at the membrane surface to the concentration in the bulk feed solution [13]. CP formation increases the salt concentration on the membrane sufrace

and thus increases the osmotic presssure across the membrane which decreases the effective driving force of the separation. As CP continues to develop, more ions accumulated near the membrane that acted like an extra membrane to decrease the flux. This process can be analogous to distinct cake or gel formation of colloidal and non-Brownian particles as illustrated in Figure 6 [20] .

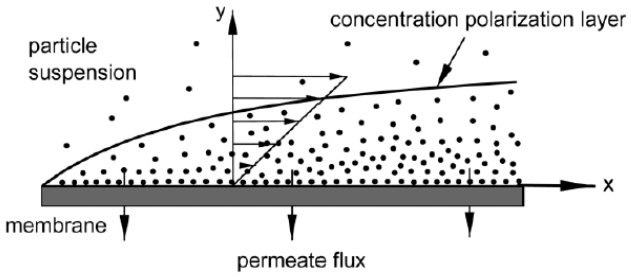

Figure 6. Cake formation of concentration polarization [20]

The rapid decrease of one specie favors the concentration build up of the other one, while the overlapping of the EDL also helps to initiate concentration polarization by charge-selective transport.

1.4 I/V Concentration polarization regimes

When the electric potentical acts as the driving force in the system, formation of CP can be observed through the current/voltage correlation where the current is used as an indicator of ion flux. As shown in Figure 7, initially the current and voltage fellow an ohmic relationship until a plateau region is reached, when the source side of membrane, which has a diffusion limit due to the CP region, blocks any further ion transport, resulting no increase of ion current even with higher applied voltage [21]. This limiting current indicates the CP formation that hinders the ion transport. After further increases to the applied voltage, significant amount of over-limiting current can be observed.

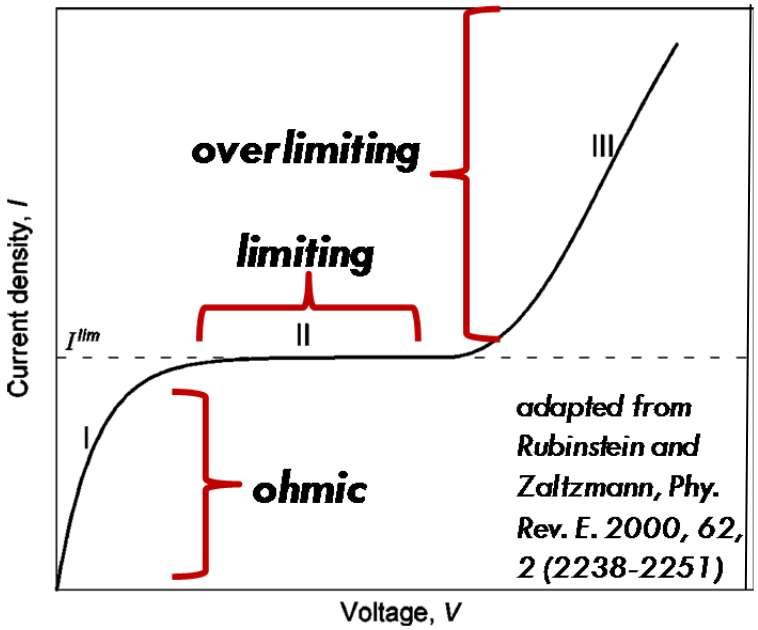

Figure 7. I/V curve indicating concentration polarization [10]

The overlimiting region indicates that specific mechanism occurs to overcome the CP. Rubinstein *et al.* suggested that convective mixing may be responsible for this phenomenon [22]. Electroconvection in strong electrolytes refers to both "*the action of the electric field upon the residual space charge of a locally quasi-electroneutral electrolyte with non-uniform concentration" and the "convection induced by electro-osmotic slip*" [22] . These mechanisms may evoke complex circular vortices allowing better mixing and permitting CP diminution [10]. However, the slope in the over-limiting region is different from that of the Ohmic region suggesting that while CP may be lower but not completely eliminated. Furthermore, an alternate hypothesis relates to the fact that at high enough potential, electrokinetic migration that the electric field induced ions transportation begins to dominate flow and causes ionic flow. Past work with membranes and CP evaluated regions similar to electrodialysis membranes or nanofluidic devices with operational potentials ranging from 1 volt to several 10s of volts [21]. Under such potentials, charge transfer or Faradaic reactions including electrolysis of water is also a significant factors that may cause the current/voltage behavior described by Rubistein. So far,

no work has been reported in the sub-1V regions where Faradaic reactions is eliminated completely for electrokinetic flow with respect to CP.

Therefore, the purpose of this thesis is to identify CP regimes under low DC bias applied (sub-1V). By identifying these regimes, methods for mitigation of CP under low potential operation can be found to achieve better efficiency in small scale desalination device.

2. Experimental Methods

2.1 Nanocapillary Array Membrane (NCAM)

NCAMs are polymeric membranes that contain large area densities of either conical or cylindrical nanopores of high length-to-diameter aspect ratios [23] [24]. Normal pore size varies from 8 nm – 100 nm [25]. The experiments were conducted by using track etched, Polyvinylpyrrolidone (PVP) coated polycarbonate membranes (diameter 25 mm) with nominal pore sizes 10 nm, 50 nm, and 100 nm (GE Osmonics) [10] Membrane pore densities and scaling to the number of pores for the open area tested are summarized in Table 2 based on the data provided by the NCAM manufacturer. A scanning electron microscope (SEM) image in Figure 8 gives an example of an NCAM membrane for a 100 nm pore size.

Table 2. Properties of nanocapillary array membrane [10]

Pore Diameter	Pore Density (pores/cm^2)	Total Number of Pores
10 nm	6.0E+08	1.2E+09
50 nm	6.0E+08	1.2E+09
100 nm	4.0E+08	8.0E+08

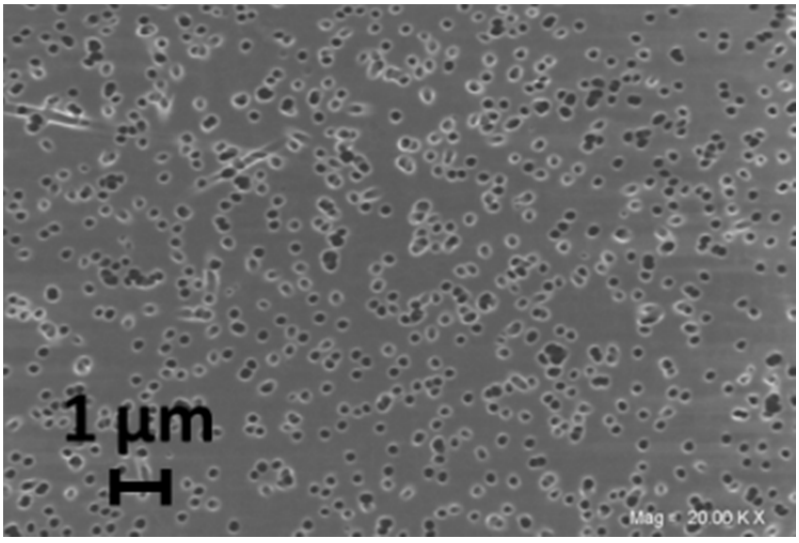

Figure 8. **SEM picture of 100nm NCAM** [10]

2.2 Experimental setup

Membranes were pre-treated by soaking in deionized water for 24 hours and then in potassium phosphate buffer for 2 hours. Potassium phosphate buffer was selected for study because it is easy to control and maintain the pH by using the Henderson-Hasselbach equation

$$\boldsymbol{pH = pK_a + log\frac{[base]}{[acid]}} \quad (5)$$

The pH was controlled because of the membrane surface charge dependence on pH, a variable which in past work had been seldom controlled [15]. High/low pH indicates basic/acid environment where excess OH^-/H^+ interacts with the surface functional groups from polymer to protonated/deprotonated and thus makes surface carried positive/negative charge. Potassium phosphate buffer fixed the pH at 7 ± 0.2 was prepared with Millipore 18.2 MΩ deionized water and monobasic and dibasic potassium phosphate salts (Sigma Aldrich, USA). The concentration would be varied from 0.2 mM, 1 mM, and 10 mM.

The ion transportation with applied bias would occur in the custom cast acrylic permeation cell shown in the Figure 9 under earth grounded Faraday cage. [10]

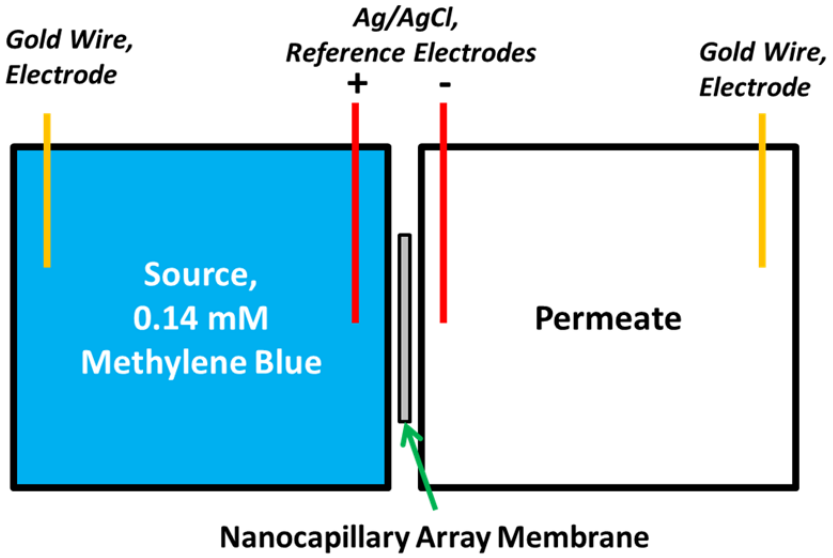

Figure 9. Schematic diagram of experimental setup [10]

Initially, the source side and the permeate side cells contain the same amount of buffer solution of 500 mL while 0.14 mM methylene blue (MB) was added to the source side. In order to induce electrokinetic flow, DC bias was applied by gold electrodes (Alfa Aesar) which was SC-1 and potentiostat (Gamry Reference 600). The voltages tested were 0 mV, 10 mV, 75 mV, 100 mV, 250 mV, 500 mV, 750 mV. MB worked as a color dye of ions and thus form concentration gradients in the source side and under the influence of electric potential, ions would transport across the nanopores to the permeate side.

Current was recorded by a potentiostat (Gamry Reference 600) throughout the whole experiment period of 60 minutes. In addition, equal volume samples were collected from both the source and permeate sides at 8 min, 15 min, 30 min, 45 min and 60 min for optical measurement.

2.3 Data analysis

2.3.1 Concentration-absorbance calibration

UV-Vis spectroscopy (Thermo-Scientific Evolution 300) was utilized for optical measurement that converted the absorbance data to concentration. The concentration variation was determined by light absorbance at 665 nm [26]. From the Beer-Lambert law that converts measured transmissivity to concentration,

$$\boldsymbol{T = \frac{I}{I_o} = 10^{-\varepsilon c l}} \tag{6}$$

where T is the transmissivity, I is the intensity of transmitted light, Io is the intensity of the incident light, ε is the absorption coefficient of the substance, and l is the distance the light travel through. Relationship between absorbance and intensity of light can be described by

$$\boldsymbol{A = -log_{10}(\frac{I}{I_0})} \tag{7}$$

Combining Equations 6 and 7, absorbance can be related to concentration by

$$\boldsymbol{A = \varepsilon c l} \tag{8}$$

where l is fixed by UV-Vis while the only unknown here is ε, a constant determined from calibration curve of each buffer concentration. Linear relationship of absorbance and concentration was utilized to construct the calibration curve. Since the buffer solution is colorless, MB is the only component that cause light absorbance change. Seven specific MB concentration buffers were prepared for absorbance testing. The results are shown in Figures 10, 11, and 12.

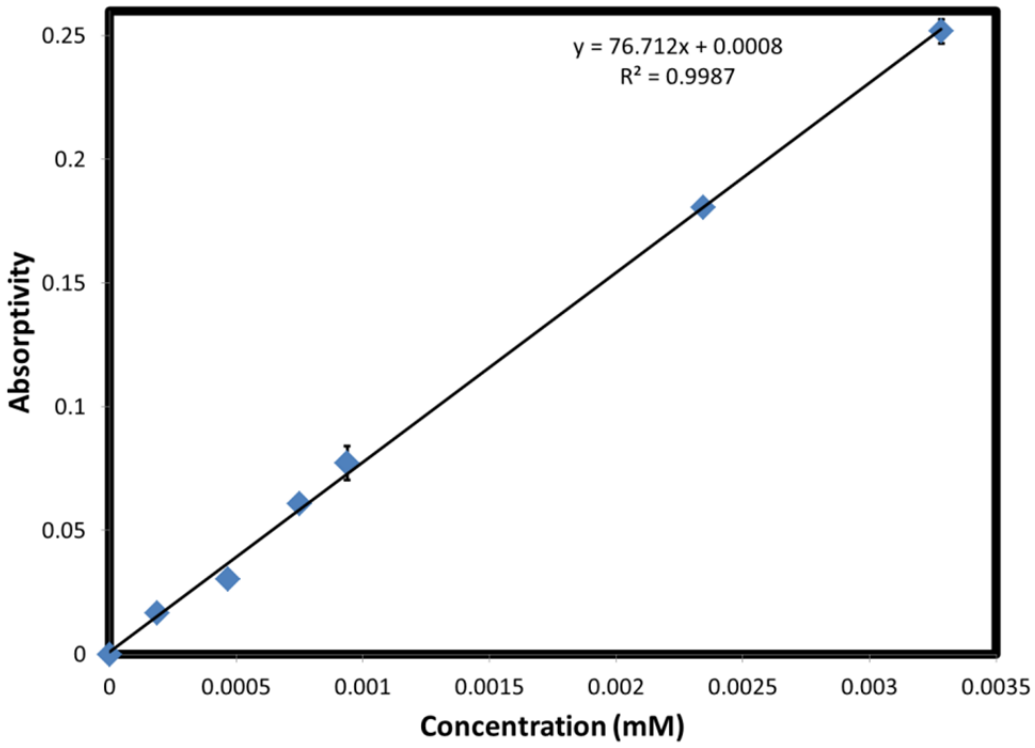

Figure 10. Calibration curve of permeate side at 0.2 mM buffer, 650 nm wavelength [10]

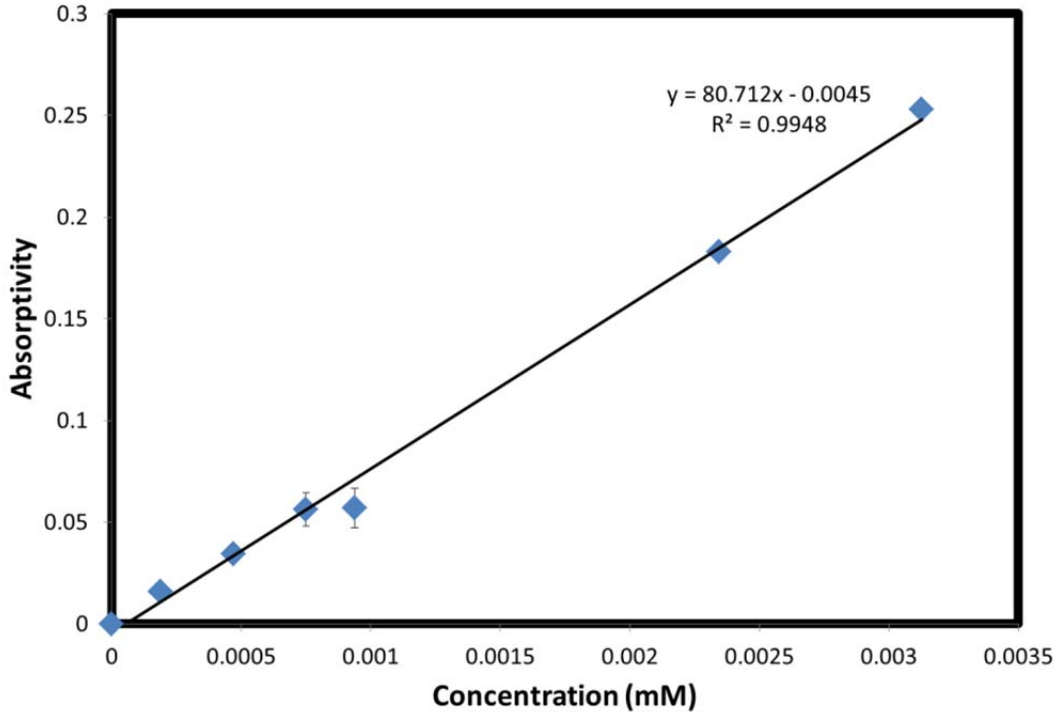

Figure 11. Calibration curve of permeate side at 1 mM buffer, 650 nm wavelength [10]

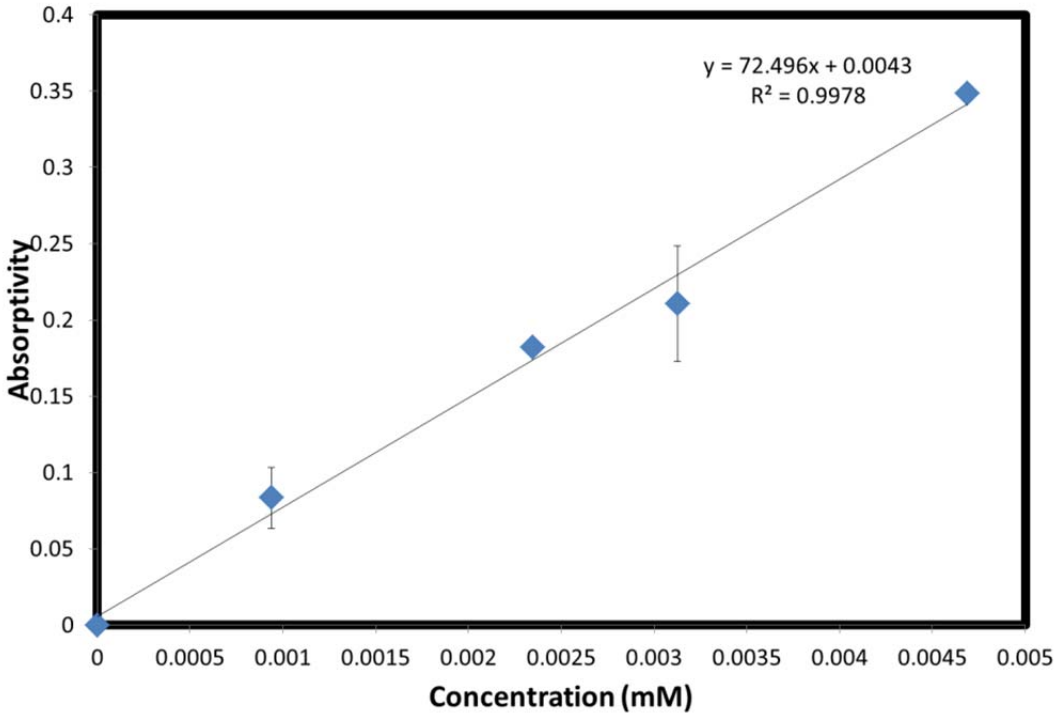

Figure 12. Calibration curve of permeate side at 10 mM buffer, 650 nm wavelength [10]

Using Figures 10-12, corresponding concentration for a certain absorbance value directly extracted from UV-Vis instrument measurement can be found.

2.3.2 Concentration-current calculation

Methylthioninium chloride (MB) is assumed to be 100% ionized to methylthioninium cations and chloride anions in the solution. The absorbance change of permeate side sample is indicated by methylthioninium cations migrating through membrane pores from source side since other ions in the solution are colorless. In addition, effect of water hydrolysis is neglected since water dissociation occurs at 1.2 V while the maximum operational DC bias applied was 0.75 V.

Current was defined as the change of charges in term of time.

$$\boldsymbol{I = \frac{\Delta Q}{\Delta t}} \tag{9}$$

Concentration gradient is defined as change of concentration in term of time, where concentration can also be interpreted as the number of MB cations in the solution per volume.

$$\boldsymbol{\frac{\Delta C}{\Delta t} = \frac{\Delta n_{particle}}{N_A * V * \Delta t}} \tag{10}$$

N_A is the Avogadro constant, and V is the volume of permeate side solution. Since MB cations carried single electron charge, the number of particle is replace by the number of electrons as

$$\boldsymbol{\Delta n_{particles} = \frac{\Delta Q}{e}} \tag{11}$$

Where *e* is the unit charge and estimated as 1.6×10^{-19} coulomb. Combining equations 9, 10 and 11, the current is related to the measured concentration gradient by equation 12.

$$\boldsymbol{I = \frac{\Delta c}{\Delta t} * (e * N_A * V)} \tag{12}$$

Error analysis is conducted by calculating the standard deviation. For each specific case, for example, 10 mm buffer, 10 nm pore size at 10 mV bias, 6 samples were collected for a certain time interval described in the experimental setup. The deviation is defined as

$$\boldsymbol{\sigma} = \sqrt{\frac{\sum_{i=1}^{6}(I_i)^2}{6} - \left(\frac{\sum_{i=1}^{6} I_i}{6}\right)^2} \tag{13}$$

where I_i is current from each sample.

2.3.3 Average current calculation

The data of current over time was recorded for each case. Average current is calculated by numerical integration with trapezoidal rule [27]. Since the data is discrete and collected over non-uniform intervals, Matlab code is modified to include x vector of time variables to the y vector of corresponding current value to allow for sufficient accuracy,

$$\boldsymbol{I(f) = \int_a^b f(t)dx \approx \frac{1}{2}\sum_{i=1}^{N}[f(t_i) + f(t_{i+1}](t_{i+1} - t_i)} \tag{14}$$

$$\boldsymbol{I_{avg} = \frac{I(f)}{t}} \tag{15}$$

where t is time. Notice that when DC bias was applied across the membrane, cations such as PO_4^{3-}, $H_2PO_4^-$ and HPO_4^{2-} moved to the cathode and anions such as K^+, H^+ MB^+ moved to the anode. The actual current is defined as the charge difference between the charges from cations to the anode through membrane and charges from anions to the cathode through membrane. The 10 mM case has ~100 times higher concentration of buffer compared to 0.14 mM MB, and thus the number of phosphate ions may greatly deviate the actual current value from the "current" describe above. In this case, normalization of the actual data by using Equation 16 in terms of number of MB ions is a proper adjustment for accurate analysis.

$$\boldsymbol{I_{MB} = I_{ave} \times \frac{n_{MB}}{n_{MB} + n_{K+} + n_{H_2PO4^-} + n_{HPO_4^{2-}} + n_{cl^-}}} \tag{16}$$

For error analysis, t-distribution is used to determine the deviation for the uneven distribution nature of current data over time that more data was collected in the beginning [28],

$$\boldsymbol{D = \pm t_{\alpha} \frac{S}{\sqrt{n}}} \tag{17}$$

Where t_{α} is extracted from student t-distribution table with 95 % of probability and 102 degree of freedom, S is the standard deviation of Equation 13 and n is the number of data collected which is 103 in the experiment.

3. Results & Discussion

3.1 Current/voltage plot from concentration

Current-voltage relations of the 10 mM buffer concentration for different nanopore sizes are plotted in Figure 13. For the same bias applied, 100 nm pore size membrane has the highest measured current among all three cases. Based on the experimental method discussed in Chapter 2.3.2 that the UV-Vis spectroscope only detects the MB ions migration, therefore 100 nm membrane pores transport the highest amount of MB cations.

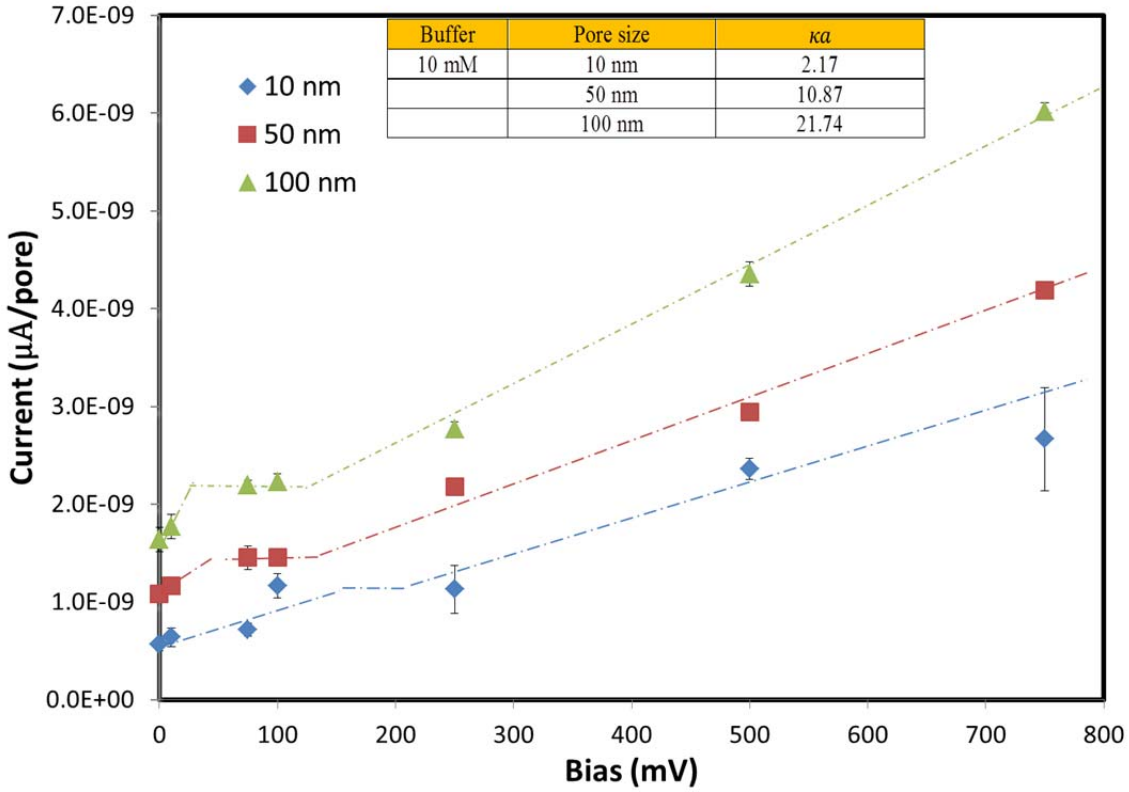

Figure 13. I/V curve based on concentration data for 10 mM buffer normalized for pore density of NCAMs, CP regime is similar to those previous reported. The CP onset of limiting and overliminting voltage described by Rubinstein was found decreasing as pore size increasing.

In addition, the general data point trend follows the pattern of CP regime discussed in Chapter 1.4 for 10 nm, 50 nm and 100 nm cases. The 10 nm membrane, for example, ohmic

relationship is observed until approximately 160 mV where a limiting current region is reached. Then the voltage starts to increase again after 210 mV. The starting voltage for both limiting and overlimiting current decreases as membrane pore size increases. Since $\boldsymbol{\kappa a}$ is larger than 1, no EDL overlapping is expected for all three cases. Larger pore size membrane allows more ions transport and thus favoring the initiation of concentration polarization at low applied bias.

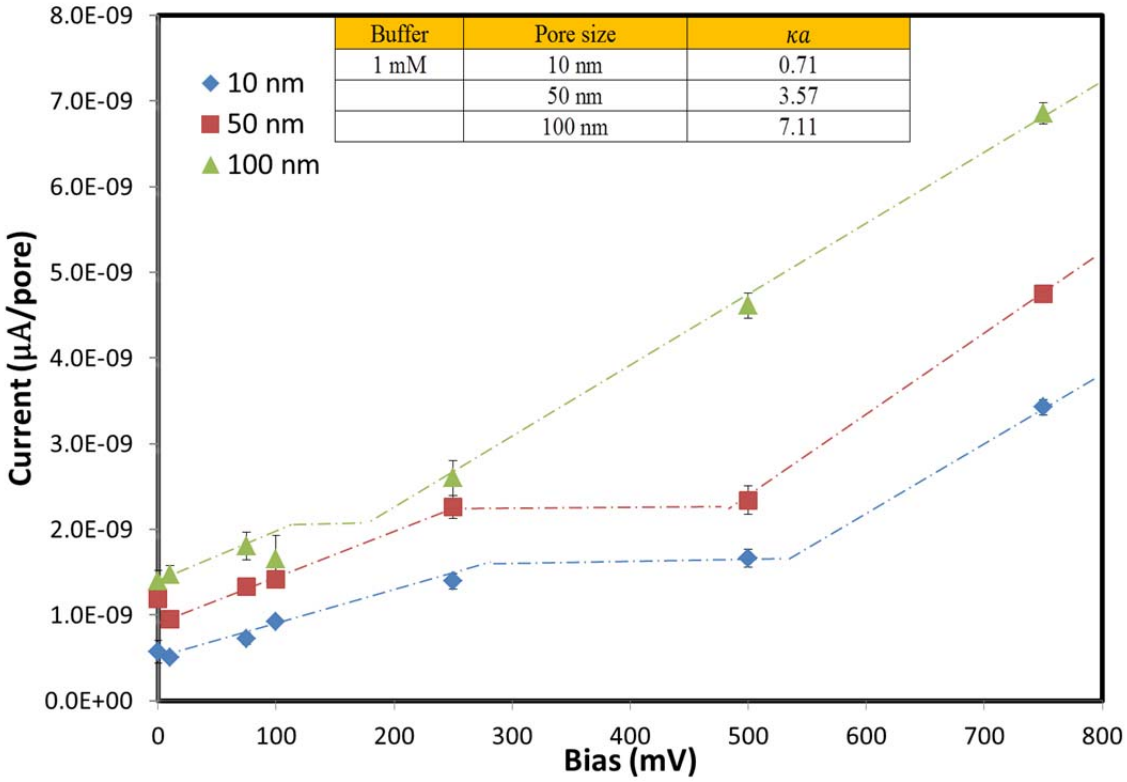

Figure 14. I/V curve based on concentration data for 1 mM buffer normalized for pore density of NCAMs, CP regime is similar to those previous reported. The CP onset was found decrease as pore size increases

The current-voltage relations of the 1 mM buffer concentration cases are shown in Figure 14. These cases also follow the major characteristic observed for the 10 mM cases and general CP regime described by Rubinstein discussed in Chapter 1.4. The current-voltage relations for the 0.2 mM buffer concentration cases are shown in Figure 15. These cases still follows the major characteristics described for the 10 mM cases and general CP regime patterns are also

observed except for the missing ohmic current for the 50 nm case. The experimental conditions, such as buffer concentration, become harder to control as buffer concentration decreases to 0.2 mM. As a result, the 0.2 mM case may experience more deviation than that of 1 mM and 10 mM cases.

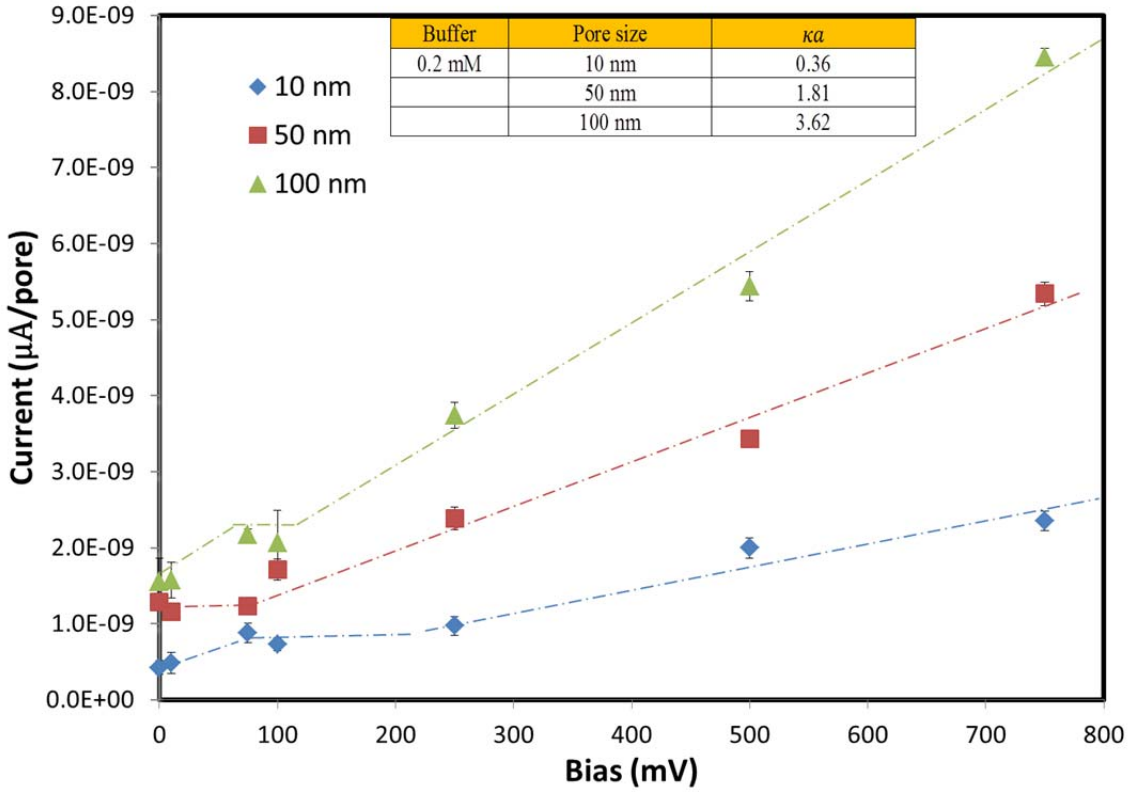

Figure 15. I/V curve based on concentration for 0.2 mM buffer normalized for pore density of NCAMs, CP regime is not similar to those previous reported. Ohmic regions are missing for 50 nm. The overlimiting regions start from ~250 mV, ~80 mV and 100 mV corresponding to the increase of pore size.

The effect of buffer concentration on the membrane current voltage relationship for the 10 nm membrane is presented in Figure 16. Identical CP regime can be observed as discussed earlier this chapter. For the same membrane pore size, the initial voltage values for limiting and overlimiting current are increasing as the buffer concentrations go down from 10 mM to 1 mM. Interestingly, 0.2 mM case did not follow this general trend and CP regime tends to occurred at

small voltage. Similar characteristic can also be observed for other membrane pore size such as 50 nm and 100 nm case in Appendix A.

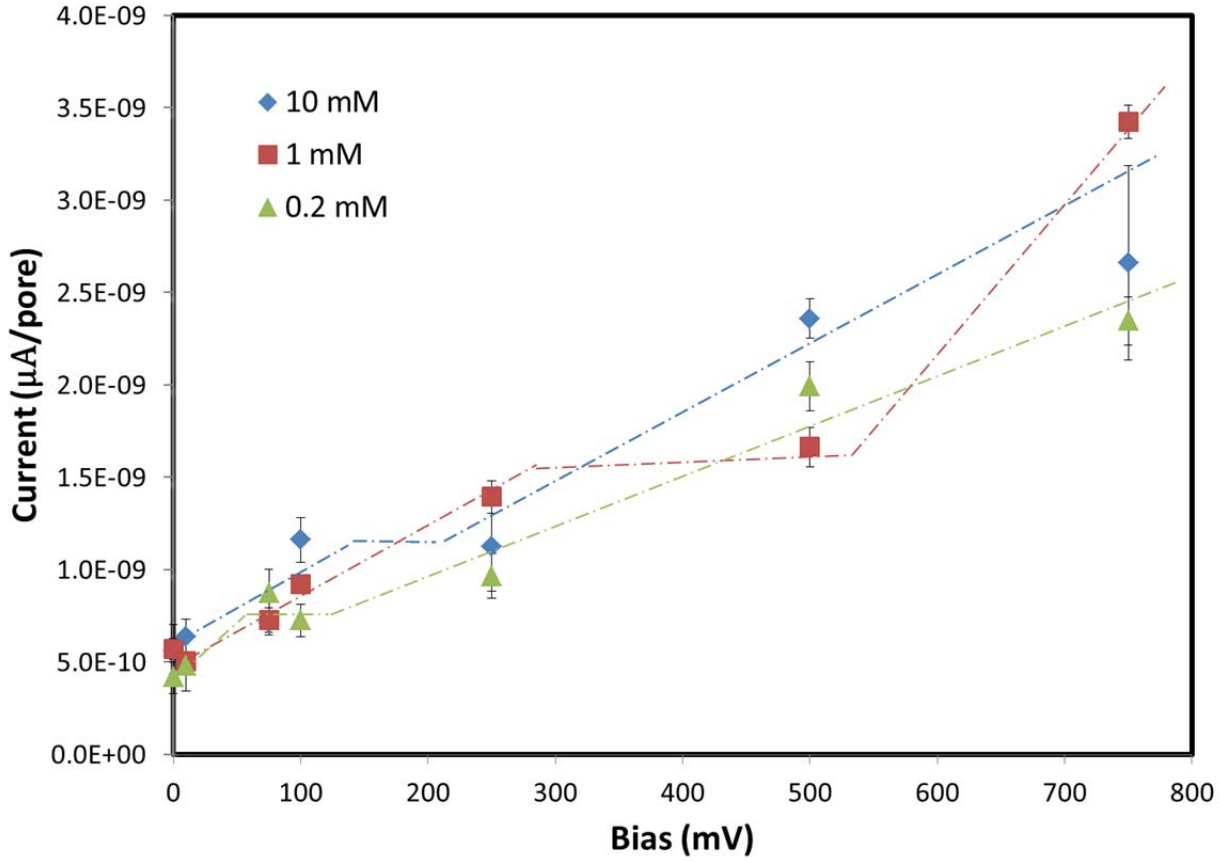

Figure 16. I/V curve for 10 nm membrane normalized for pore density. CP regime observed here is described in Figures 13-15.

3.2 Current/voltage plot by Potentiostat

The current-voltage relations for the 10 mM case, based on the current data normalized for number of MB ions, are plotted in Figure 17. It can be shown that pore sizes have no effect on the current voltage relationship. All the data points of the same voltage almost overlap with each other considering the error bar presented. This indicates that membrane pore size have no effect on the amount of current that can passes through them, which is not consistent with what has been discussed in Chapter 3.1.

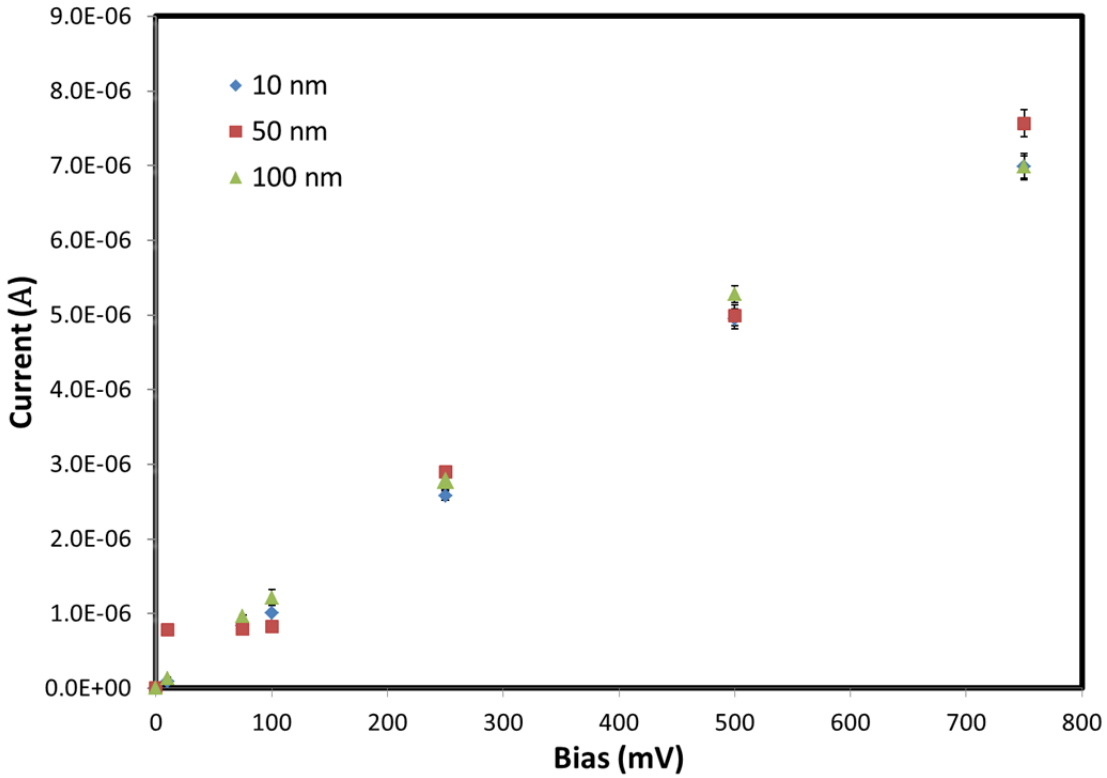

Figure 17. I/V curve based on current for 10 mM buffer solution. The data points indicate a linear relation with all three pore size data points overlapping at the same applied voltage

Beside the possible experimental device deviation, the actual current value may be deviated by other important factors such as resistance of the membrane as well as the capacitance of the EDL inside the membrane pores [10]. Recall the previous assumption that MB cations migration from the source side to the permeate side contribute to the only source of current for studying the CP regime (Chapter 2.3.2). However, Potentiostatic machine reports the current of the whole system in which contains the membrane, ions and EDL inside the pores. As a result, the reported current result may not reflect the ion transport properly because of the parallel and series circuit relationship in Figure 18. Beyond this thesis, more accurate circuit analysis should be conducted to minimize the influence of membrane resistance and capacitance of EDL. Therefore, all the analysis of current data will be inconclusive and beyond the scope of this thesis.

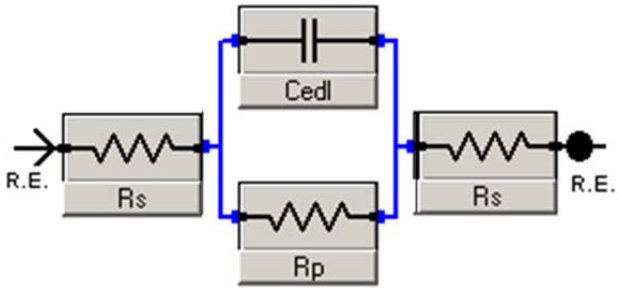

Figure 18. Proposed equivalent circuit model for NCAM including the membrane solution interface. Note Rs is solution resistance, Cedl is the capacitance of the EDL in the pore and Rp is the resistance of the pore [10]

As summarize below in Table 3, for 10 mM buffer concentration, where no overlapping exist, the onset regime decreases as pore size increases. EDL overlap for $\kappa\alpha$ = **0.71** of 1 mM, 10 nm membrane still follows the general trend of the voltage required for limiting region, as those of non-overlapping one. Although electrokinetic flow dominates the overall transport mechanism, its effect to the onset CP regime is not great enough compared to the pore size. For $\kappa\alpha$ = **0.36** of the 0.2 mM, 10 nm membrane, the over-limiting current is even lower than that of the 100 nm one. The effect of EDL clearly exceeds the effect of the pore diameter. Therefore, it is possible that there is a point of $\kappa\alpha$ between 0.36 and 0.71 that the effect of pore size and EDL overlap counteracts with each other.

Table 3. Summery of $\kappa\alpha$ [10] and estimated voltage to start limiting and overlimiting current region

			Concentration Data	
Concentration (mM)	Pore (nm)	$\kappa\alpha$	limiting current	over-limiting current
10	10	2.17	160	210
	50	10.9	50	140
	100	21.7	30	120
1	10	0.71	280	530
	50	3.56	250	490
	100	7.11	110	190
0.2	10	0.36	80	210
	50	1.81	0	80
	100	3.62	75	120

4. Conclusions

The concentration polarization regime that described by Rubinstein of ohmic, limiting and over-limiting current is clearly observed for most of the parameters tested except for the 0.2 mM, 50 nm case. In addition, the study of parameters such as membrane pore size and buffer concentration show that with same buffer solution concentration, as pore size increases, the system has a higher current and the onset of CP regime also has a decreasing voltage value. For the same pore size membranes, the onset of CP regimes has an increasing voltage value as buffer concentration goes up.

For future work recommendations, optimization of the current data to get more representative current value by eliminating the system impedance is necessary to improve the current data and get more accurate results. This can be done by testing only the membrane with or without buffer solution as a reference point for each parameter sets.

Reference

[1] U.S. Department of Energy, "Energy Demands on Water Resources: Report to Congress on the Interdependency of Energy and Water," 2006.

[2] National Intergrated Drought Information System, "U.S dought monitor," 2012.

[3] "World population," http://census.gov/population/international, extracted from internet on July 12th, 2012.

[4] Veolia Inc., "Finding the Blue Path for A Sustainable Economy," Veolia Water North America, Chicago, IL, 2010.

[5] R. Service, "Desalination freshens up," *Science,* vol. 313, pp. 1088-1090, 2006.

[6] E. Delyannis, "Historic background of desalination and renewable energies," *Solar Energy,* vol. 75, no. 5, pp. 357-366, 2003.

[7] T. Hillie and M. Hloph, "Nanotechnology and the challenge of clean water," *Nanotechnol,* vol. 2, p. 663, 2007.

[8] L. F. Greenleea, D. F. Lawlerb, B. D. Freemana and B. Marrotc, "Reverse osmosis desalination: Water sources, technology," *Water Research,* vol. 43, pp. 2317-2348, 2009.

[9] M. Shannon, P. Bohn and M. Elimelech, "Science and technology for water purification in the coming decades," *Nature,* vol. 452, p. 301, 2008.

[10] K. Bellman, "Identification of Low potential Onset of Concentration Polarization and Concentration Polarization Mitigation in Water Desalination Membrane," The Ohio State University, 2011.

[11] D. Hasson and R. Semiat, "Scale control in saline and wastewater desalination," *Israel Journal of Chemistry,* vol. 46, pp. 97-104, 2006.

[12] A. Kumari, G. Sarkhel and A. Choudhury, "Preparation and Characterization of Polyvinylpyrollidone Incorporated Cellulose Acetate Membranes for," *Jornal of Applied Polymer Science,* pp. Volume 124, Issue S1, 2012.

[13] C. Geankoplis, "Membrane separation process," in *Transport processes and seperation process principle* , NJ: Prentice Hall, 2009.

[14] R. Baker, "Membrane technology and application," Chichester, England, John Wiley & Sons, 2004.

[15] S. Prakash, A. Piruska, E. Gatimu and et.al., "Nanofluidics: Systems and Application," *Sensors Journal, IEEE,* vol. 8, no. 5, pp. 441-450, 2008.

[16] P. Adrien, B. Schoch and P. Renaud, "Ionic Transport Phenomena in Nanofluidics: Experimental and Theoretical Study of the Exclusion-Enrichment Effect on a Chip," *Nano Letter,* vol. 5, no. 6, pp. 1147-1155, 2005.

[17] D. Li, Electrokinetics in Microfluids, Oxford, GBR: Academic Press, 2004.

[18] N. Kaushik, Membrane separation processes, New Delhi: Prentice Hall, 2008.

[19] T. Pedley, "Calculation of Unstirred Layer Thickness in Mmeber Transport Experiments," vol. 16, no. 2, 1983.

[20] J. Chen, Q. Li and E. M, "In situ monitoring techniques for concentration polarization and fouling phenomena in membrane filtration," vol. 107, 2004.

[21] S. Kim, Y. Wang, J. Lee and J. han, "Concentration polarization and nonlinear electrokinetic flow near a nanofluidic," *Physical Review Letter,* vol. 99, pp. 044501-1 to 044501-4, 2007.

[22] I. Rubinstein and B. Zaltzman, "Electro-osmotically induced converction at a permselective membrane," *Physics Review,* vol. 62, no. 2, pp. 2238-2251, 2000.

[23] S. Prakash, J. Yeom, N. jin, I. Adesida and M. Shannon, "Characterization of Ionic Transport at the Nanoscale," *Journal of Nanoengineering and Nanosystem,* vol. 220, pp. 45-52, 2007.

[24] S. Prakash, M. Pinti and K. Bellman, "Variable cross-section nanopores fabricated in silicon nitride membranes using a transmission electron microscope," *Journal of Micromechanics and Microengineering,* vol. 22, 2012.

[25] D. Fung, E. Akdemir, M. J. Vitarelli, S. Sosnov and S. Prakash, "Transport of Charged Species across Solid-State Nanopores," *Materials Research Socociey Symposium Proceedings,* p. 1139, 2009.

[26] O. (. M.J, The Merck Index: An Encyclopedia of Chemicals, Drugs, and Biologicals, 14th ed, NJ: Merck, 2006.

[27] D. Cruz-Uribe and C. J. Neugebauer, "Sharp Error Bounds for the Trapezoidal Rule and Simpson's Rule," *Journal of Inequialities in Pure and Applied Mahematics,* vol. 3, no. 4, 2002.

[28] J. L. Devore, "The one-Sample t confidence interval," in *Probability and Statistics for Engineering and the Sciences*, Belmont, Thomson Higer Education, 2008, p. 272.

Appendix A: Current voltage relationship of fixed nanopore size with comparison of influence of buffer concentration to the concentration polarization regime. Similar characteristic discussed in Chapter 3.1 can be observed here.

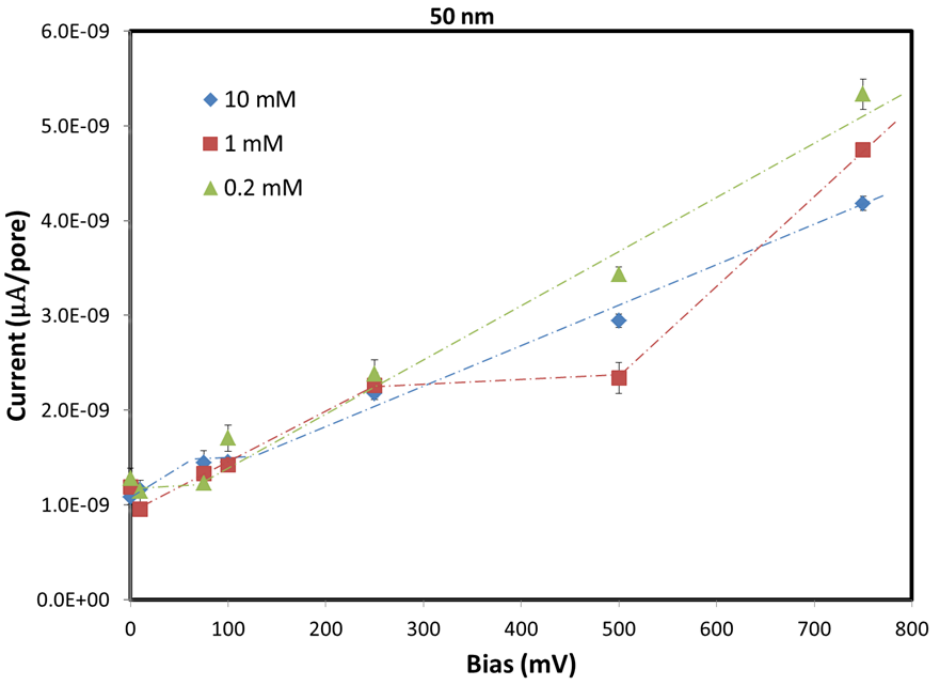

Appendix A1. I/V curve for 50 nm membrane normalized for pore density. CP regime observed here is described in Figures 13-15

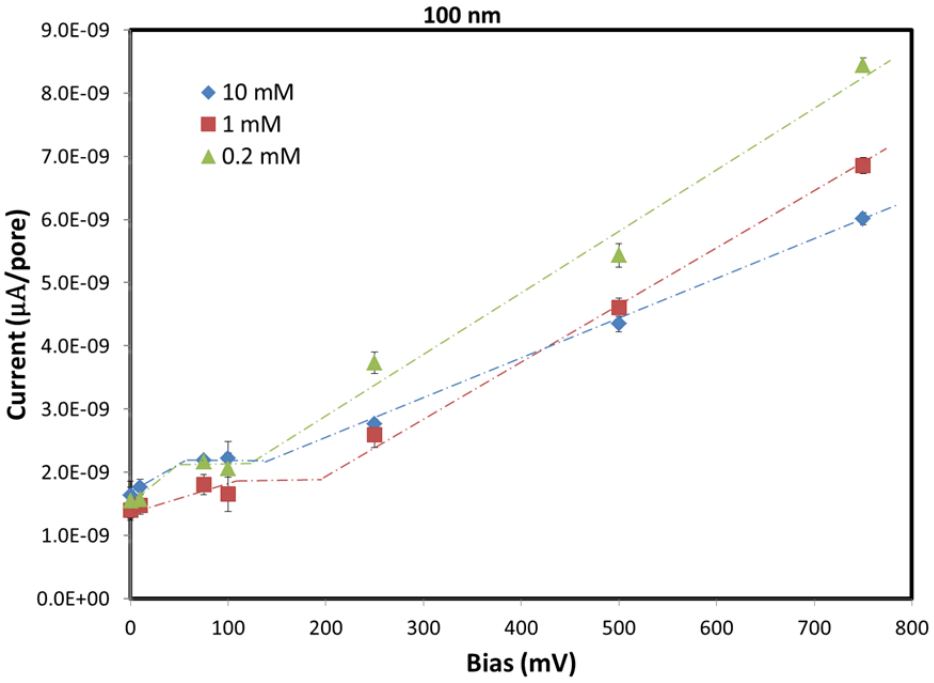

Appendix A2. I/V curve for 100 nm membrane normalized for pore density. CP regime observed here is described in Figures 13-15

Appendix B: Current voltage relationship of fix buffer concentration for comparison of nanopore size towards the CP regime. Below are the Figures from current data which are inconclusive considering the potential error discussed in Chapter 3.2 and beyond the scope of study of this thesis. 10 mM case is within the Chpater.

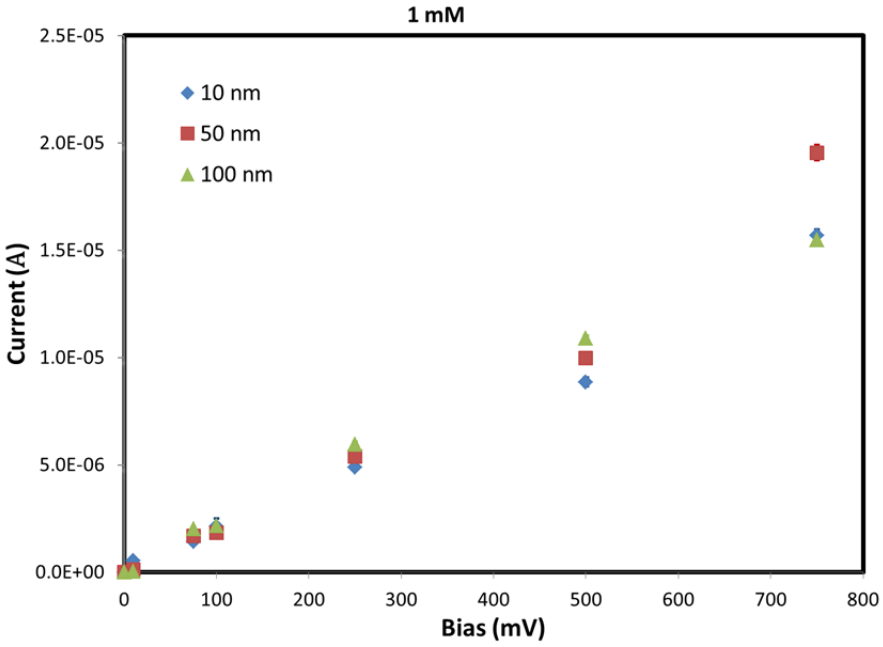

Appendix B1. I/V curve based on current for 1 mM buffer solution

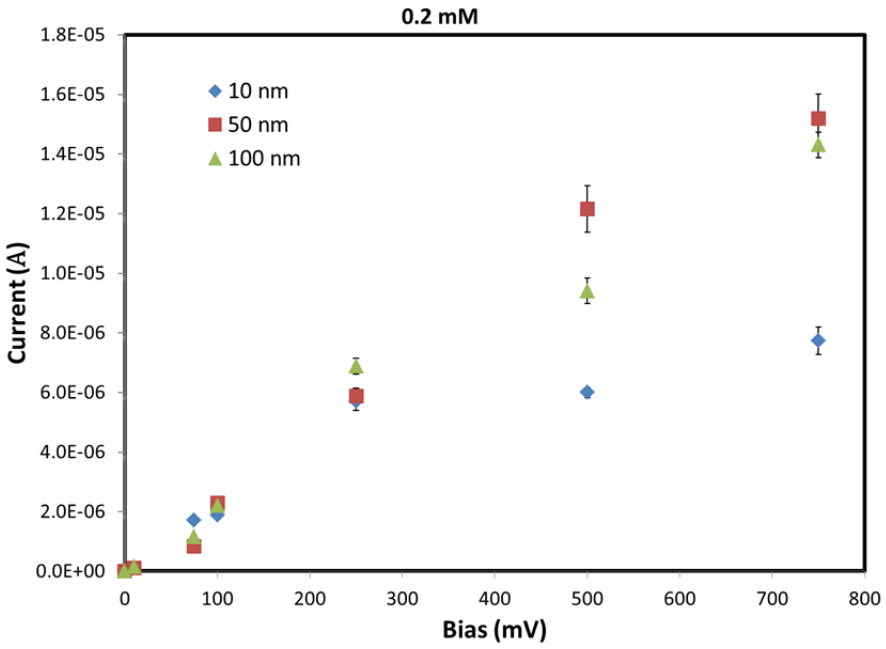

Appendix B2 I/V curve based on current for 0.2 mM buffer solution

Appendix C: Current voltage relationship of fix nanopore size for comparison of buffer concentration towards the CP regime. Below are the Figures from analysis of current data which are not conclusive considering the potential error discussed in Chapter 3.2 and beyond the scope of study of this thesis.

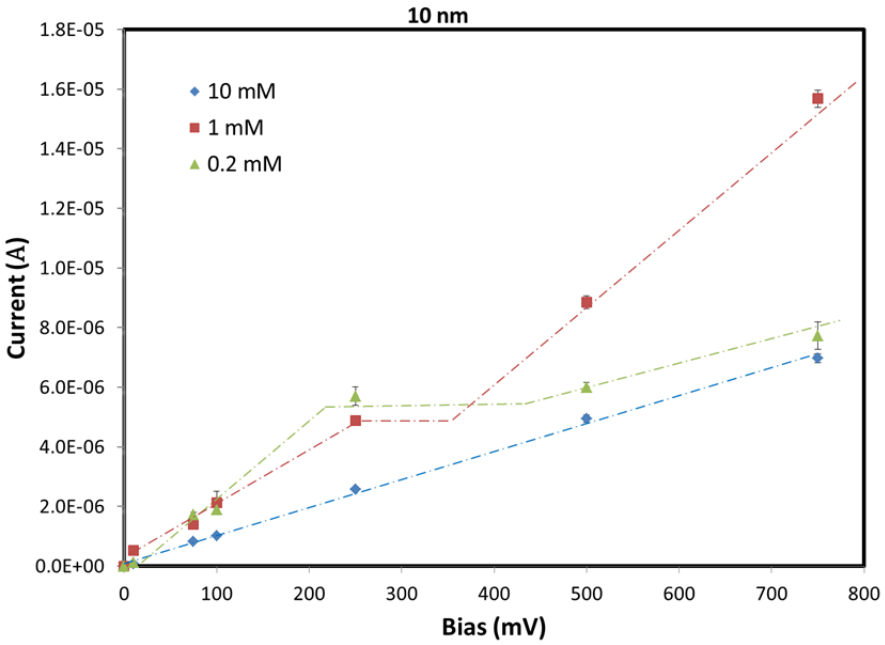

Appendix C1: I/V curve based on current for 10 nm NCAM pore size

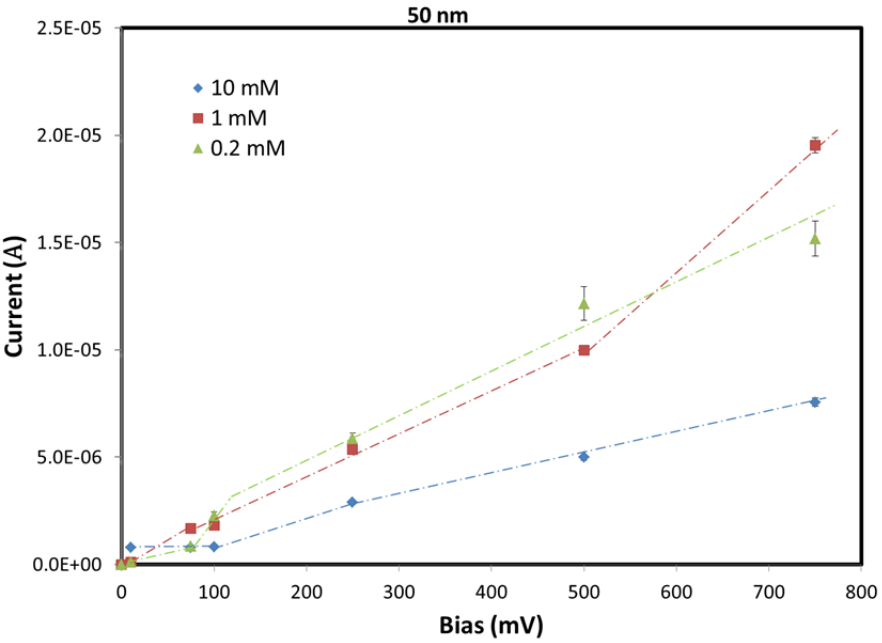

Appendix C2. I/V curve based on current for 50 nm NCAM pore size

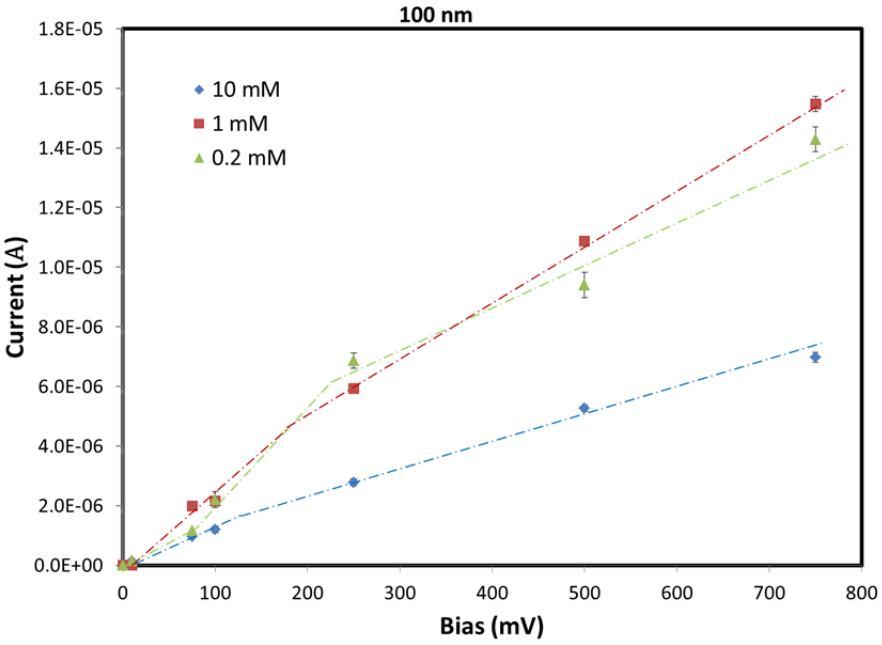

Appendix C3. I/V curve based on current for 100 nm NCAM pore size